Lateralization of temporal lobe epileptic foci with automated chemical exchange saturation transfer measurements at 3 Tesla

Kang Wang,[a,f] Qingqing Wen,[b,f] Dengchang Wu,[a] Yi-Cheng Hsu,[c] Hye-Young Heo,[d] Wenqi Wang,[b] Yi Sun,[c] Yuehui Ma,[e] Dan Wu,[b] and Yi Zhang[b,*]

[a]Epilepsy Center, Department of Neurology, First Affiliated Hospital, College of Medicine, Zhejiang University, Hangzhou, Zhejiang, 310003, China
[b]Key Laboratory for Biomedical Engineering of Ministry of Education, Department of Biomedical Engineering, College of Biomedical Engineering & Instrument Science, Zhejiang University, Hangzhou, Zhejiang, 310027, China
[c]MR Collaboration, Siemens Healthcare Ltd., Shanghai, 201318, China
[d]Division of MR Research, Department of Radiology, Johns Hopkins University School of Medicine, Baltimore, MD, USA
[e]Epilepsy Center, Department of Neurosurgery, First Affiliated Hospital, College of Medicine, Zhejiang University, Hangzhou, Zhejiang, 310003, China

eBioMedicine
2023;89: 104460
Published Online xxx
https://doi.org/10.1016/j.ebiom.2023.104460

Summary

Background Magnetic Resonance Imaging (MRI) is an indispensable tool for the diagnosis of temporal lobe epilepsy (TLE). However, about 30% of TLE patients show no lesion on structural MRI (sMRI-negative), posing a significant challenge for presurgical evaluation. This study aimed to investigate whether chemical exchange saturation transfer (CEST) MRI at 3 Tesla can lateralize the epileptic focus of TLE and study the metabolic contributors to the CEST signal measured.

Methods Forty TLE subjects (16 males and 24 females) were included in this study. An automated data analysis pipeline was established, including segmentation of the hippocampus and amygdala (HA), calculation of four CEST metrics and quantitative relaxation times (T_1 and T_2), and construction of prediction models by logistic regression. Furthermore, a modified two-stage Bloch–McConnell fitting method was developed to investigate the molecular imaging mechanism of 3 T CEST in identifying epileptic foci of TLE.

Findings The mean CEST ratio (CESTR) metric within 2.25–3.25 ppm in the HA was the most powerful index in predicting seizure laterality, with an area under the receiver-operating characteristic curve (AUC) of 0.84. And, the combination of T_2 and CESTR further increased the AUC to 0.92. Amine and guanidinium moieties were the two leading contributors to the CEST contrast between the epileptogenic HA and the normal HA.

Interpretation CEST at 3 Tesla is a powerful modality that can predict seizure laterality with high accuracy. This study can potentially facilitate the clinical translation of CEST MRI in identifying the epileptic foci of TLE or other localization-related epilepsies.

Funding National Natural Science Foundation of China, Science Technology Department of Zhejiang Province, and Zhejiang University.

Keywords: Chemical exchange saturation transfer imaging; Lateralization; Temporal lobe epilepsy; Molecular imaging mechanism; Elevated amine

Introduction

Epilepsy is one of the most common neurological disorders, affecting about 1 in 100 people worldwide.[1] Persistent seizures can cause various problems, such as brain injury and psychosocial disabilities, severely affecting patients' health and quality of life.[2] Temporal lobe epilepsy (TLE) is the most common subtype of epilepsy, accounting for up to 40% of all epileptic cases.[3] The vast majority of TLE (>80%) originates in the mesial temporal lobe, i.e. in and around the hippocampus.[4]

*Corresponding author. Room 322, Zhou Yiqing Building, Yuquan Campus, Zhejiang University, 38 Zheda Road, Hangzhou, 310027, China.
E-mail address: yizhangzju@zju.edu.cn (Y. Zhang).
[f]Kang Wang and Qingqing Wen contributed equally to this study.

Research in context

Evidence before this study

Magnetic Resonance Imaging (MRI) is one of the mostly-used diagnostic tools for temporal lobe epilepsy (TLE). However, about 30% of TLE patients show no abnormal manifestation on the structural MR images, which complicates the preoperative evaluation and is associated with worse surgical outcomes. A prior study has shown that glutamate chemical exchange saturation transfer (CEST) at 7 T is a useful modality for predicting seizure laterality of patients with non-lesional TLE. However, only 4 subjects were included in the study, and 7 T MRI is not uniformly available, which hindered its clinical translation. There has been no follow-up clinical application by any other group since the initial 7 T CEST work, which reflected both the difficulty of the methodology and the unsuccessful translation.

Added value of this study

In this study, we demonstrated that CEST imaging at 3 Tesla is able to localize the hemisphere containing the epileptic network in 40 TLE patients, regardless of the presence or absence of lesions on the patient's structural MR images. And a two-stage Bloch–McConnell fitting method revealed that the increased amine and guanidinium moieties might be the molecular source of 3 T CEST in detecting epileptic foci.

Implications of all the available evidence

CEST imaging can provide a valuable noninvasive biomarker for diagnosing TLE preoperatively. Amine protons, such as in glutamate, might be the molecular source for the image contrast detected between epileptic foci and normal tissues. Since 3 T MRI scanners are ubiquitous in imaging centers, the CEST technology can potentially be adopted for clinical TLE evaluation rapidly.

About 1/3 of TLE patients are refractory to the anti-convulsive drug therapy, for whom surgical resection is often performed to control the seizures.[5]

Magnetic Resonance Imaging (MRI) is an indispensable tool for identifying epilepsy-related structural lesions. Patients with discernible lesions that can be depicted by structural MRI usually have better post-operative outcomes than those without lesions.[6] However, about 30% of TLE patients show no lesion on conventional MR images, which are typically defined as "MRI-negative" cases,[7] or should be termed "structural-MRI-negative" ("sMRI-negative") to be more precise. The absence of lesions undermines the etiological diagnosis of epilepsy and the preoperative evaluation of patients referred to resection surgery. Generally, the presurgical localization of the non-lesional epileptogenic zone is complex and time-consuming, but it is key to successful surgery.[8,9]

Advanced MRI sequences can play a vital role in detecting epileptic foci, and have been applied in multiple studies, including diffusion tensor imaging (DTI) and magnetic resonance spectroscopic imaging (MRSI).[10–13] In a DTI study, Concha et al. reported that the mean diffusivity of the fiber tracks that carry connections of the temporal lobe could correctly lateralize 87% of the 24 TLE patients using linear discriminant analysis.[10] Another DTI study by Pustina et al. showed that the fractional anisotropy of the inferior longitudinal fasciculus yielded an accuracy of 70.7% in predicting the laterality of epileptogenic foci.[11] In an MRSI study by Knowlton et al., the ratio of the concentration of N-acetylaspartate and that of combined choline and creatine correctly lateralized 61% of the 23 patient cohort,[12] while in another study from Capizzano et al., an accuracy of 80% was reported using the right-left asymmetry index of the N-acetylaspartate signal intensity.[13] Despite the promising results, these existing advanced MRI methods have not been successfully translated into routine clinics yet. Thus, novel MRI sequences are urgently needed to assist the lateralization of the epileptogenic zone.

Chemical exchange saturation transfer (CEST) imaging is an emerging MRI technique that can detect proteins and metabolites noninvasively through the exchange of protons between biomolecules and free water.[14,15] The exchange rate of amine protons in glutamate is in the slow to intermediate exchange regime (~2000–~5000 s^{-1})[15–18] with respect to its chemical shift at 7 T (~5600 rad/s), making glutamate an ideal target metabolite for CEST detection at 7 T or higher field strength. Notably, glutamate plays a crucial role in the generation and maintenance of seizures, as demonstrated by both human[19] and animal[20] studies. A recent study at 7 T[6] found that glutamate CEST imaging could localize the hemisphere containing the epileptic network by detecting the elevated glutamate level in the hippocampus of patients with TLE. But, there were only 4 TLE patients in this preliminary study, and 7 T scanners are not uniformly available,[6] which hindered its translation into routine clinical use. In contrast, 3 T MRI scanners are ubiquitous in the clinic globally. However, as the exchange rate of amine protons in glutamate is in the intermediate to fast exchange regime versus its chemical shift at 3 T (~2400 rad/s), whether CEST at 3 T can label amine protons to detect the epileptic foci in TLE needs to be investigated. A latest study demonstrated successful detection of tubers in patients with epilepsy secondary to the tuberous sclerosis complex using 3 T CEST and suggested that amine protons might be the major contributor to the elevated CEST signal in tubers.[18] Thus, we hypothesize that CEST MRI can predict seizure laterality of TLE at 3 T.

Here, CEST MRI at 3 T was applied to TLE patients. A relatively large cohort of 40 unilateral TLE subjects was enrolled to explore the feasibility of 3 T CEST in predicting epileptic laterality. Automated brain segmentation and data processing were achieved to obtain the CEST index values in the hippocampus and amygdala regions. Then the CEST indices at various saturation frequencies were used to build the laterality prediction models by the logistic regression method. The optimal CEST index and the corresponding saturation frequency were determined with the receiver-operating characteristic (ROC) analysis. Finally, we endeavored to expound the imaging mechanism of 3 T CEST in identifying epileptic foci of TLE.

Methods

Study design

This prospective study aims to investigate the feasibility of CEST MRI at 3 Tesla in lateralizing the seizure foci of TLE. The experimental design is shown in Fig. 1A. First, MRI images of multiple modalities (source CEST and relaxation time mapping images) were acquired for each TLE subject, with the corresponding index maps (CEST metric and relaxation time maps) obtained after data post-processing. Second, the hippocampus and amygdala were segmented automatically on the three-dimension (3D) T_1-weighted (T_1w) images and then registered to the two-dimension (2D) target CEST or relaxation source image, so that the index values in the hippocampus and amygdala could be automatically calculated. Third, logistic regression was used to build the prediction model using the quantitative CEST and relaxation indices, and the ROC analysis was used to evaluate the performance of each index in epileptic lateralization. Finally, we attempted to explain the metabolic mechanism of CEST signals at 3 T in differentiating epileptic lesions and normal tissues using a modified two-stage Bloch–McConnell fitting method.[18]

Subjects

Forty-eight TLE subjects were consecutively recruited from May 2019 to January 2021. As shown in Fig. 2, the inclusion criteria of patient enrollment were: i) The patient had no prior history of brain surgery and no contraindication for MRI scanning; ii) Epileptic symptoms, scalp video electroencephalogram (EEG) readings, and neuropsychological patterns were consistent with the characteristics of mesial temporal lobe epilepsy proposed by the International League Against Epilepsy[21]; iii) Except epilepsy-related abnormalities, there were no other structural changes on anatomical MR images; iv) Unilateral temporal lobe epilepsy was reported by the epileptologists. The exclusion criteria of patient enrollment were: i) The patient was diagnosed with non-mesial TLE epilepsy, such as neocortical temporal lobe epilepsy; ii) The CEST or relaxation mapping data was incomplete. A total of 40 mesial TLE patients (16 subjects with right

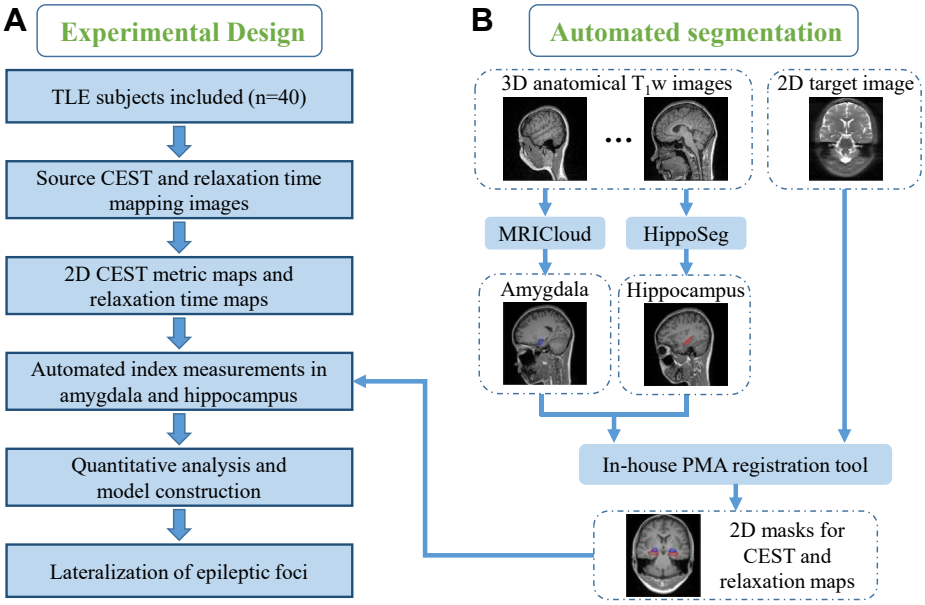

***Fig. 1:* Workflow of laterality prediction using automated CEST and relaxation measurements.** (A) Experimental design. MRI data of 40 unilateral TLE patients were acquired. After automatically obtaining CEST and relaxation indices in the target anatomy, the laterality prediction model was constructed by logistic regression. (B) Hippocampus and amygdala were segmented from the 3D anatomical T_1w images by MRICloud and HippoSeg tools, respectively. Then, the 3D T_1w images were registered to the 2D CEST or relaxation image using the in-house position matching algorithm (PMA) tool, with the 2D hippocampus and amygdala masks generated automatically.

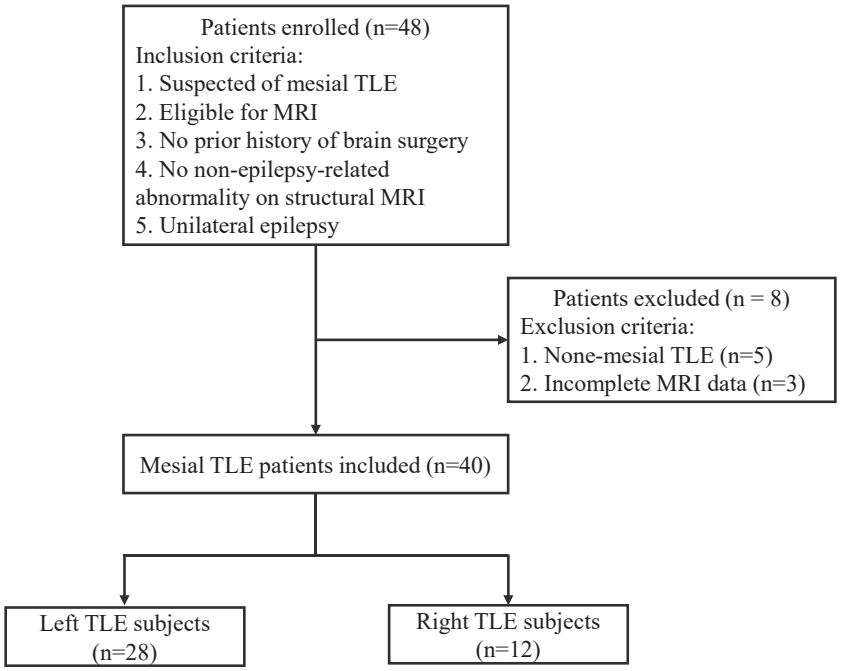

Fig. 2: **The flow diagram of patient selection.**

TLE and 24 cases with left TLE; age range: 14–51 years old; 16 males and 24 females) were included. The lateralization of epileptic foci was mostly based on a comprehensive workup, including clinical and neurologic examinations, ictal scalp video-EEG recordings, anatomical T_1w and T_2-weighted (T_2w) brain MRI, and optional brain PET scans. Two epileptologists (with 16 and 11 years of clinical experience, respectively) made the decision of the epileptic focus laterality by a consensus analysis of the comprehensive data described above. For a small group of patients (n = 5), temporal lobectomy was performed, and the laterality was determined based on intracranial stereo-electroencephalography (SEEG) and clinical outcomes (Supplementary Table S1).

Ethics statement

This prospective study was approved by the institutional review board of the First Affiliated Hospital of Zhejiang University in Zhejiang, China (reference no. IRB2017-326). Before the MRI experiments, written informed consent from each patient or parental guardian was obtained.

MRI acquisition

MRI acquisition was performed on a 3 Tesla scanner (MAGNETOM Prisma, Siemens Healthcare, Erlangen, Germany). MRI protocols included T_1w magnetization-prepared rapid gradient echo (MPRAGE),[22] T_2w fluid-attenuated inversion recovery (FLAIR),[23] CEST, B_0 mapping water saturation shift referencing (WASSR),[24] T_1 mapping inverse recovery (IR), and T_2 mapping multi-echo spin-echo (MESE) sequences. The key parameters of the 3D MPRAGE sequence were: repetition time (TR) = 2.3 s, echo time (TE) = 2.3 ms, field of view (FOV) = 240 × 240 × 172.8 mm^3, resolution = 0.9 × 0.9 × 0.9 mm^3, and duration = 5.4 min. As for the 3D FLAIR sequence, the main acquisition parameters were: TR = 5 s, TE = 387 ms, time of inversion (TI) = 1.8 s, FOV = 230 × 230 × 172.8 mm^3, resolution = 0.9 × 0.9 × 1.1 mm^3, and duration = 5.7 min. Anatomical images acquired from the MPRAGE and FLAIR sequences were used to locate the coronal hippocampal plane for single-slice CEST, WASSR, IR, and MESE scans. The CEST data were acquired using a 2D turbo spin-echo (TSE) readout[25] with the following parameters: TR/TE = 5000/8.1 ms, FOV = 212 × 185.5 mm^2, resolution = 1.0 × 1.0 mm^2, slice thickness = 5 mm, radiofrequency (B_1) field saturation power = 4 μT (35 patients) or 3 μT (5 subjects), B_1 saturation duration = 1000 ms, 62 saturated frames at frequencies from –6 to 6 ppm stepped at 0.25 ppm plus 15.6 ppm as well as one unsaturated reference frame, and duration = 5.4 min. In addition, for a subgroup of 14 patients, extra CEST data with a B_1 power of 1 μT were acquired to facilitate the subsequent two-stage Bloch–McConnell fitting. The spatial location, FOV, resolution, and slice thickness of WASSR, IR, and MESE scans were the same as those used in the CEST sequence. Other key parameters of the WASSR scan were: TR/TE = 2000/8.1 ms, B_1 = 0.5 μT, B_1 saturation time = 200 ms, 26 saturation frequencies = –1.5 to 1.5 ppm stepped at

0.125 ppm, and duration = 56 s. As for the IR scan, notable parameters were: TR/TE = 3000/8.1 ms, TI = 50, 150, 300, 500, 800, 1300, and 2000 ms, and duration = 47 s. The major parameters of the MESE scan were: TR = 500 ms, TE = 12–192 ms stepped at 12 ms, and duration = 1.6 min.

CEST and relaxation metric calculation

MATLAB (MathWorks, Natick, MA, USA) was used for the post-processing of the MRI data. For each voxel, the WASSR z-spectrum was fitted by a 12th-order polynomial, and the difference between the frequency of the fitted minimum value and 0 Hz was taken as the B_0 offset. Then, the raw CEST z-spectrum was shifted according to the B_0 offset to obtain the final B_0-corrected z-spectrum. Four CEST metrics were calculated from the z-spectra,[26] i.e.

$$CESTR(\Delta\omega) = [S(-\Delta\omega) - S(\Delta\omega)] \,/\, S_0 \quad \text{Equation. (1)}$$

$$CESTR^{nr}(\Delta\omega) = [S(-\Delta\omega) - S(\Delta\omega)] \,/\, S(-\Delta\omega) \quad \text{Equation (2)}$$

$$MTR_{rex}(\Delta\omega) = [S(-\Delta\omega) - S(\Delta\omega)] \cdot S_0 \,/\, [S(-\Delta\omega) \cdot S(\Delta\omega)] \quad \text{(Equation (3)}$$

$$AREX(\Delta\omega) = MTR_{rex} / T_1 \quad \text{Equation (4)}$$

where Δω represents the saturation frequency offset, $S(\Delta\omega)$ is the saturated signal at Δω, and S_0 is the unsaturated signal. For each of the four CEST metrics, 20 indices at various frequencies were obtained, including those at single frequencies within 1∼4 ppm stepped at 0.25 ppm, and those from mean values for frequency ranges of 2∼4, 2.25∼3.75, 2.5∼3.5, 2.75∼3.25, 2∼3, 2.25∼3.25, and 2.25∼2.75 ppm. T_1 maps were calculated from the IR data by a 3-parameter exponential fit of $y = a - b \cdot e^{-TI/T_1}$, where y is the acquired data, and a, b and T_1 are the unknown values to be determined. T_2 maps were computed from the MESE data using a 2-parameter exponential fit of $y = c \cdot e^{-TE/T_2}$, with c and T_2 as the unknown values.

Automated index measurements

Fig. 1B shows the procedures of automated mask generation. The hippocampus was automatically segmented from the 3D T_1w image volume using HippoSeg,[27,28] a tool specifically for hippocampal segmentation of epilepsy patients (http://niftyweb.cs.ucl.ac.uk/). And the amygdala was automatically segmented by MRICloud[29] (https://mricloud.org/). A multiplanar reconstruction from the 3D T_1w images (and the associated hippocampus and amygdala masks) to the 2D target CEST/relaxation image was achieved with an in-house position matching algorithm (PMA) tool. The PMA software utilized the spatial coordinate information recorded in the image header and generated images matching the spatial location, FOV, and resolution of the target one. The reconstructed 2D hippocampus and amygdala masks were then eroded by eliminating the voxels with values < 0.6. In total, six regions of interest (ROIs) were obtained for each subject, with three in each hemisphere: (i) hippocampus, (ii) amygdala, and (iii) hippocampus plus amygdala (HA). For each ROI, a total of 82 index measurements were automatically generated, including 20 values for each of the four CEST metrics as described above, and T_1 and T_2 values. Two asymmetry measures were used to discriminate the left and right TLE groups: difference asymmetry measurement M_1 = I (left) - I (right) and ratiometric asymmetry measurement M_2 = [I (left) - I (right)]/[I (left) + I (right)], where I represents the index value.

Two-stage Bloch–McConnell fitting

A two-stage analysis method[18] was adopted and modified to analyze the leading metabolic contributor in the epileptogenic HA compared with the normal HA. The two-stage analysis used data from 7 subjects that were scanned with two B_1 saturation powers of 1 μT and 4 μT, and had relatively large differences in the CESTR spectrum between the ipsilateral HA and the contralateral HA. In the first stage, the CESTR spectra in the normal HA were fitted according to a 7-pool Bloch–McConnell model. The starting values were taken from a prior report,[18] as shown in Supplementary Table S2. The boundaries of the pool size and exchange rate were [0.5, 2] and [0.5, 1.5] times the starting values, respectively. The resonant frequency, T_1 and T_2 of each exchangeable CEST pool were fixed, and T_1 and T_2 of the water pool were obtained from the IR and MESE sequences described above. A total of 12 variable parameters, including the concentration/pool size (f_i) and exchange rate (k_i) of the ith ($1 \le i \le 6$) CEST pool, were generated and fed into the next stage as starting values.

In the second stage, the 6 exchangeable pool sizes were varied to simulate the contrast between CESTR spectra in the epileptogenic HA and those in the normal HA. Only one pool size was allowed to vary each time, with the other parameters fixed at values from the first stage. For each run of the BM simulation, the pool size was swept from 20% to 500% (stepped at 1%) of the starting value. The root mean squared error (RMSE) was used to assess the agreement of the simulated and experimental CESTR contrasts, with the CESTR contrast = CESTR (epileptogenic HA) – CESTR (normal HA). For each pool, the minimum RMSE (mRMSE) and

the corresponding concentration change were obtained. A smaller mRMSE indicated a high possibility that the corresponding metabolite may have caused the CEST contrast between the epileptogenic and normal HA.

Statistics

Statistical analyses were performed using MATLAB and SPSS (IBM SPSS Statistics, Armonk, NY, USA). Paired *t*-test was used to compare the difference between indices. Logistic regression was used to build the prediction model of each single index, and stepwise multivariate logistic regression was used to select and combine indices. The area under the curve (AUC) values obtained from receiver-operating characteristic (ROC) analysis were used to evaluate the predictive ability of each model. The optimal index for differentiating the right TLE (RTLE) from the left TLE (LTLE) was obtained by comparing the AUC values.

Role of the funding source

The sponsors of this study had no role in the study design, data collection, analysis, interpretation, or writing of the paper.

Results

The clinical characteristics of included patients are displayed in Supplementary Table S1, all of whom were retained in the final analysis, including 16 males and 24 females. The mean age was 34.88 years for all the patients (standard deviation: 10.48 years; range: 14–51 years). Eleven TLE patients showed no lesion on conventional MRI and were determined to be structurally normal by radiologists blinded to the study. Besides, a patient (P01) with RTLE was misidentified as a LTLE case based on structural MRI. These 12 patients were collectively referred as "sMRI-negative" cases. Five patients (P01, P08, P17, P19, and P30) underwent surgical treatment, and the intracranial SEEG and clinical outcomes verified the preoperative localization of the epileptic foci by the epileptologists. For each patient, a total of 82 index maps were obtained after data post-processing, including two quantitative relaxation (T_1, T_2) maps and 20 maps (at different saturation frequencies) for each of the four CEST metrics (CESTR, $CESTR^{nr}$, MTR_{rex}, AREX). Notably, the quantitative relaxation maps revealed the source of image contrast seen on structural MRI, and the different CEST metrics were used to shield various contaminants from the target CEST effect.[26] As shown in Fig. 1, the in-house PMA tool can reconstruct a 2D structural T_1w image along with hippocampus and amygdala masks matching the location and resolution of the 2D CEST or relaxation image from 3D structural T_1w images, which enables automatic calculation of CEST and relaxation indices in the target ROIs.

Lateralization performance of CEST indices from hippocampus and amygdala in all patients

Table 1 shows the maximum AUC of each CEST metric and the corresponding optimal saturation frequency in differentiating LTLE from RTLE. The AUCs of quantitative T_1 and T_2 were also listed for comparison. It can be found that the mean CESTR index within 2.25–3.25 ppm was the best predictor among all the single indices tested, with an AUC value of 0.84 for both difference (M_1) and ratiometric (M_2) asymmetry measurements between left and right HA, which was much higher than the classification accuracy of the radiologists (AUC = 0.65). Unlike the CESTR metric, the maximum AUC values of $CESTR^{nr}$, MTR_{rex}, and AREX occurred at different saturation frequencies for the M_1 and M_2 asymmetry measurements, and the M_2 index (AUC = 0.77, 0.73, and 0.72, respectively) all outperformed M_1 (AUC = 0.67, 0.66 and 0.70, respectively). For the index at the optimal frequencies, paired *t*-test revealed significant differences in CESTR, T_1, and T_2 between the ipsilateral HA to the epileptic focus and the contralateral HA ($p \leq 0.01$), while not for MTR_{rex} or AREX. The optimal $CESTR^{nr}$ performance evaluated for M_1 occurred within 2.25–3.25 ppm, with a significant difference observed between the epileptogenic and normal HA ($p = 0.049$), while that calculated for M_2 (at 1.5 ppm) did not reach a significant level ($p = 0.50$). The maps of T_1, T_2, CESTR, $CESTR^{nr}$, MTR_{rex}, and AREX from a representative LTLE patient are shown in Supplementary Fig. S1.

Index	M_1				M_2			
	Frequency	AUC	95% CI	*P*	Frequency	AUC	95% CI	*p*
T_1	/	0.74	[0.58, 0.90]	0.01	/	0.74	[0.58, 0.90]	0.01
T_2	/	0.77	[0.62, 0.93]	<0.01	/	0.78	[0.63, 0.93]	0.03
CESTR	2.25–3.25 ppm	0.84	[0.72, 0.97]	<0.01	2.25–3.25 ppm	0.84	[0.71, 0.97]	<0.01
$CESTR^{nr}$	2.25–3.25 ppm	0.67	[0.50, 0.84]	0.07	1.5 ppm	0.77	[0.63, 0.92]	<0.01
MTR_{rex}	3.5 ppm	0.66	[0.50, 0.83]	0.08	1.5 ppm	0.73	[0.57, 0.89]	0.02
AREX	4 ppm	0.70	[0.53, 0.87]	0.03	1.5 ppm	0.72	[0.56, 0.88]	0.02

Both difference (M_1) and ratiometric (M_2) asymmetry measurements between the two hemispheres were evaluated for each index. The optimal frequency (range) for each CEST index, corresponding AUC, 95% confidence intervals (CI) of AUC, and *p* values of AUC were listed. CESTR yielded the best predictive accuracy in all the single indices.

Table 1: **Lateralization performance using indices from the combined hippocampus and amygdala.**

We then further evaluated the lateralization performance of single and combined metrics of T_1, T_2, and CESTR (within 2.25–3.25 ppm) for all the subjects. As shown in Fig. 3A, the signal ratio of CESTR between the epileptic HA and the contralateral normal HA was significantly ($p < 0.05$) higher than that of T_1 and T_2. Among these three metrics, stepwise logistic regression selected T_2 and CESTR as significant predictors ($p < 0.05$) for seizure laterality. Fig. 3B and C presents the ROC curves of T_1, T_2, CESTR, and the combined T_2 and CESTR metric. For a single predictor, CESTR produced higher AUC than T_1 and T_2. For the M_1 asymmetry measurement (Fig. 3B), the combination of T_2 and CESTR yielded a higher AUC of 0.92 (95% confidence interval [CI]: 0.84 to 1) than CESTR (0.84 as in Table 1) and T_2 (0.77). Similarly, for M_2 (Fig. 3C), the combined T_2 and CESTR metric generated an AUC of 0.91 (95% CI: 0.83 to 1), higher than that of T_2 (0.78) and CESTR (0.84) alone.

Fig. 4 illustrates the T_1w, T_1, T_2, and CESTR images of three sMRI-negative patients (A-C) and one sMRI-positive patient (D) determined by radiologists based on the 3D T_1w and T_2w images, respectively. The hippocampus (black lines) and amygdala (blue lines) masks were automatically overlaid onto the 2D relaxation and CEST maps by the in-house PMA tool. For the sMRI-negative patient with LTLE in Fig. 4A, both relaxation and CEST maps show higher values in the epileptogenic HA than in the contralateral HA. For the sMRI-negative patient with RTLE in Fig. 4B, higher T_1 and CESTR signals can be observed in the right HA, but it is difficult to identify the lesion laterality from the T_2 map. For the sMRI-negative subject with RTLE in Fig. 4C, the contrasts of T_1 and T_2 between left and right HA are not obvious, while the CESTR signal in the right HA is clearly higher than that in the left HA. Similarly, for the sMRI-positive case with LTLE in Fig. 4D, the elevated signal of left HA can be easily seen on the CESTR map, but not on the T_1 and T_2 maps.

Predictive power of T_1, T_2, and CESTR in sMRI-positive and sMRI-negative groups

The predictive ability of T_1, T_2 and CESTR (within 2.25–3.25 ppm) from HA was evaluated for patients with sMRI-positive (n = 28) and sMRI-negative (n = 12) findings, respectively. The AUC values and associated ROC curves are shown in Fig. 5. For sMRI-negative subjects (Fig. 5A–C), CESTR stood out as the most informative index with respect to the lateralization of the seizure onset, with AUC values of 0.83 for both M_1 and M_2 asymmetry measurements, and the accuracy of lateralization was 10/12. In comparison, the predictive power of T_1 and T_2 was much weaker (Fig. 5A). Especially, the AUC value of T_2 was close to 0.5, which indicated that T_2 was incapable of detecting the seizure laterality for the sMRI-negative subcohort. For sMRI-positive subjects (Fig. 5D–F), the abilities of CESTR and T_1 to distinguish the epileptogenic side (AUC = 0.84 and 0.73) were consistent with those in the sMRI-negative cases (AUC = 0.83 and 0.75). Notably, T_2 generated the highest AUC value of 0.87 in the sMRI-positive subgroup, which was substantially better than that in the sMRI-negative subgroup (AUC ≤0.56).

Predictive performance of T_1, T_2, and CESTR from the hippocampus or amygdala alone

As a subanalysis, we evaluated the lateralization performance of T_1, T_2, and CESTR (within 2.25–3.25 ppm) using indices calculated from the hippocampus or amygdala alone, as shown in Table 2. Two subjects were excluded because the size of the hippocampus or amygdala was less than 8 voxels, resulting in 38 patients included in the subanalysis. For both the M_1 and M_2 asymmetry measurements, the predictive power of the relaxation and CEST indices from the amygdala were all lower than those from the hippocampus. The performance of T_1 and T_2 in the hippocampus was slightly better than that in the combined HA (0.78 vs. 0.74–0.78), as in Table 2 vs. Table 1. However, for the CESTR

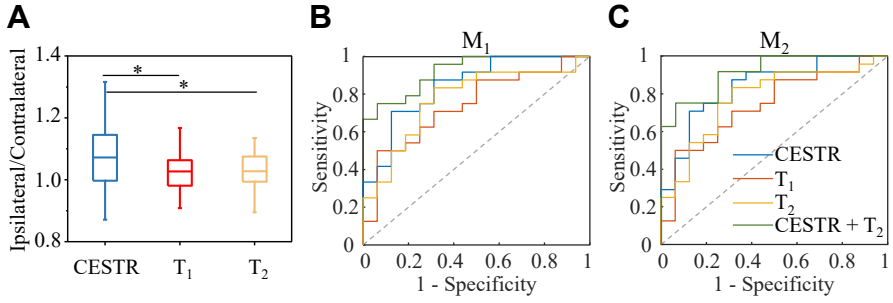

***Fig. 3:* Comparison of CEST and relaxation indices for seizure lateralization.** **(A)** Ratios of CESTR, T_1, and T_2 values in the epileptogenic HA to those in the contralateral normal HA. "*" indicates $p < 0.05$. ROC curves for the lateralization of epileptic foci using the difference asymmetry index M_1 (**B**) and ratiometric asymmetry index M_2 (**C**) in the region of HA. The ROC curves include single metrics of CESTR (within 2.25–3.25 ppm), T_1, and T_2, as well as the combined CESTR and T_2 metric. As for the single metrics, the AUC values of CESTR (blue lines) are higher than those of T_1 (red lines) and T_2 (orange lines) for both M_1 and M_2 indices. Furthermore, the combined CESTR and T_2 metric (green lines) can obtain a higher accuracy of laterality prediction than the single index.

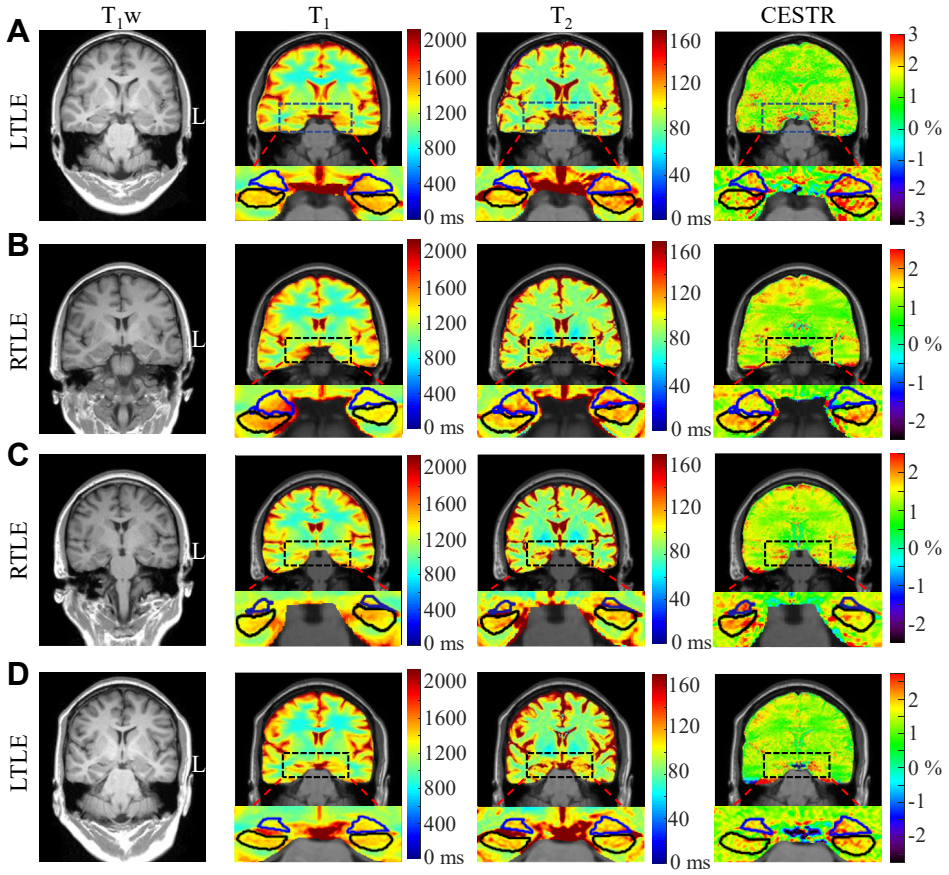

***Fig. 4*: Coronal slices of T_1, T_2, and CESTR maps along with reconstructed T_1w images from four representative TLE patients.** (**A**) For an sMRI-negative patient with left TLE (LTLE), the T_1 and T_2, and CESTR (within 2.25–3.25 ppm) maps all show higher signals in the left HA than the right one. (**B**) For an sMRI-negative patient with right TLE (RLTE), there is a visible elevation in the CESTR and T_1 signals of the right HA, but not in the T_2 signal. (**C**) An sMRI-negative RTLE patient, with a visible increase in the CESTR of the right HA. But, there is no visible difference between the left and right HA regions on T_1 and T_2 maps. (**D**) For an sMRI-positive LTLE patients, the difference between the left and right HA cannot be observed on T_1 and T_2 maps, while a marked increase in CESTR of the left HA can be found. Blue and black lines encircle the amygdala and hippocampus, respectively.

index, the values from the HA provided better prediction than either hippocampus or amygdala alone (0.84 vs. 0.73–0.82).

Potential metabolic contributors to the CEST contrast measured

Table 3A lists the fraction and exchange rate of each exchangeable CEST pool for generating the fitted CESTR spectra in the normal HA (Supplementary Fig. S2), which were output from the first stage of the two-stage analysis method. Starting from the normal Bloch–McConnell parameters in Table 3A, the effects of the six pool sizes on the CEST contrast between the epileptogenic and normal HA are shown in Table 3B and Fig. 6. The simulated spectra with a 25% increase in the amine concentration were the most consistent with the experimental results, with the smallest error as shown in Fig. 6D and Table 3B. In addition, a 34% elevation in the guanidinium pool fraction yielded the second-lowest mRMSE (Fig. 6C). These results suggest that the amine and guanidinium pools might have played a leading role in generating the CEST contrast between the epileptogenic and normal HA.

Discussion

This study investigated the feasibility of 3 T CEST in predicting TLE laterality in a relatively large sample. An automated pipeline was established to investigate the diagnostic performance of CEST indices in lateralizing TLE foci. The mean CESTR value within 2.25–3.25 ppm from the HA region was the best predictive index in distinguishing left and right TLE, with an AUC value of 0.84 which was larger than those of quantitative T_1 (0.74) and T_2 (0.78). Moreover, the combination of T_2 and CESTR further increased the AUC to 0.92. These results

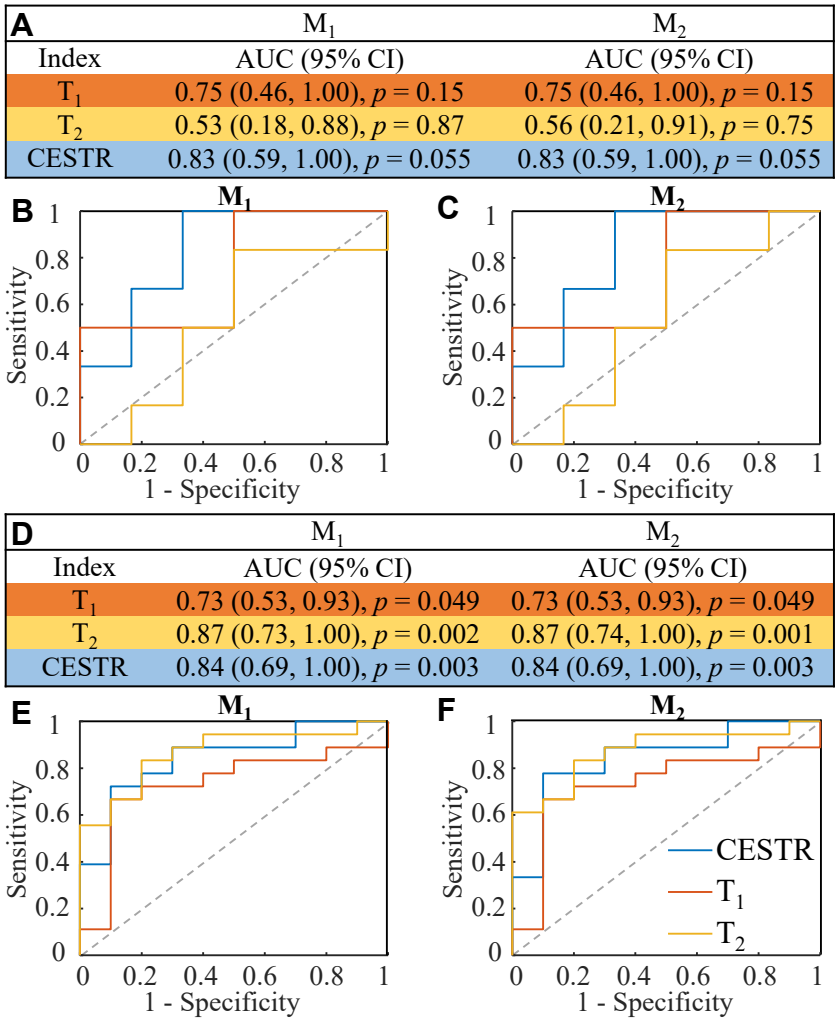

Fig. 5: **Lateralization performance of CESTR, T_1, and T_2 for the sMRI-negative (A, B, C) and sMRI-positive (D, E, F) patients. (A)** The AUCs of different metrics calculated using the difference (M_1) and ratiometric (M_2) asymmetry measurements for sMRI-negative patients, with corresponding ROC curves shown in **(B)** and **(C)** for M_1 and M_2, respectively. **(D–F)** The AUC results and associated ROC curves for sMRI-positive patients. The laterality prediction of CESTR in the sMRI-negative (AUC: 0.83), sMRI-positive (AUC: 0.84), and total (AUC: 0.84) patients is relatively stable. The laterality accuracy of CESTR in the sMRI-negative patients is much higher than that of T_1 and T_2, while for the sMRI-positive patients, T_2 is the best predictive index, with a slightly higher AUC (0.87) than that of CESTR (0.84).

indicate that CEST MRI is a potentially useful tool for preoperative lateralization of the seizure focus in TLE.

The correct diagnosis of TLE from neuroimaging data requires highly trained professionals.[11] The accuracy of epileptic lateralization usually depends on many subjective factors,[11] and different epilepsy experts may reach different laterality diagnoses with the same neuroimaging data.[30] With advanced image analysis methods, previous TLE studies using DTI[10] and T_2 relaxometry[31] have shown that the accuracy of laterality prediction by automated quantification can match or exceed that of experts' visual inspection. Since drawing ROI manually is often time-consuming, highly subjective, and difficult to reproduce,[32] automatic segmentation with established tools[27–29] has been adopted to automate the processing pipeline in this study. The best prediction model can then be obtained conveniently using the automatically-obtained indices. In addition, the CEST acquisition sequence can be easily integrated into the current MRI workflow without requiring new hardware or contrast agents. The image processing steps, including B_0 calculation from WASSR, Z-spectrum correction, CESTR computation, index extraction from hippocampus and amygdala, and establishment of the epilepsy laterality prediction model by logistic regression, can all be automated in MATLAB. Thus, the technologies used in this study should be readily translatable to other sites.

A	Hippocampus	
	M_1	M_2
Index	AUC (95% CI)	AUC (95% CI)
T_1	0.78 (0.62, 0.93), $p < 0.01$	0.78 (0.63, 0.94), $p < 0.01$
T_2	0.78 (0.63, 0.93), $p < 0.01$	0.78 (0.63, 0.93), $p < 0.01$
CESTR	0.82 (0.68, 0.95), $p < 0.01$	0.81 (0.67, 0.94), $p < 0.01$
B	**Amygdala**	
	M_1	M_2
Index	AUC (95% CI)	AUC (95% CI)
T_1	0.70 (0.53, 0.87), $p = 0.04$	0.69 (0.52, 0.86), $p = 0.05$
T_2	0.72 (0.56, 0.89), $p = 0.02$	0.72 (0.56, 0.89), $p = 0.02$
CESTR	0.73 (0.57, 0.89), $p = 0.02$	0.74 (0.59, 0.90), $p = 0.01$

The CESTR value was the mean within 2.25–3.25 ppm as in Table 1. Both difference (M_1) and ratiometric (M_2) asymmetry measurements between the two hemispheres were evaluated for each index. The AUC values of CESTR were the highest in both hippocampus and amygdala. For every index, the AUC from the hippocampus was higher than that from the amygdala. Two subjects of the total 40 patients were excluded due to the small size of the hippocampus or amygdala (<8 voxels).

Table 2: **Lateralization performance using T_1, T_2, and CESTR from the hippocampus (A) or amygdala (B) alone.**

The CESTR metric exhibited the best predictive ability among the four widely-used CEST metrics tested (Table 1), although the $CESTR^{nr}$, MTR_{rex}, and AREX metrics are often regarded to yield less contaminated signals than CESTR.[26] This is likely because some of the interfering factors are symbiotic for the diagnosis of epileptic foci, and a cleaner CEST metric does not necessarily signify a better clinical performance.[15] In any case, the molecular CEST metric outperformed the structural T_1 and T_2 metrics, regardless of whether the ROI was the combined HA or hippocampus/amygdala alone (Tables 1 and 2). For T_1 and T_2, the mean values in the hippocampus generated better AUC values than those in the combined HA, indicating that quantitative T_1 and T_2 values in the hippocampus can already provide clear evidence for seizure laterality, as reported in past TLE studies.[31,33] In contrast, the average CESTR indices in the HA exhibited slightly better AUC than those in the hippocampus or amygdala, which might be due to the greater region of abnormality detected by CEST than sMRI or the higher signal to noise ratio in the combined HA than hippocampus/amygdala alone.

In the metric calculation, the M_1 and M_2 asymmetry measurements used the contralateral side of the brain as a control for each subject, mitigating confounders from inter-person and inter-scan variations.[11] Although the ratiometric asymmetry measurement (M_2) is often used in the prediction study and is sensitive to pathology,[11,34] we found that the difference asymmetry measurement (M_1) was generally comparable to M_2 in the laterality prediction (Tables 1 and 2). Notably, the combined use of M_1 and M_2 was beneficial for selecting the robust CEST or relaxation metric. Specifically, the optimal saturation offsets of $CESTR^{nr}$, MTR_{rex}, and AREX were inconsistent between the two asymmetry measurements (Table 1), reflecting the relatively poor reliability of the laterality prediction using these indices. In contrast, T_1, T_2, and CESTR showed almost the same AUC values regardless of M_1 or M_2, and the optimal frequencies corresponding to CESTR were also consistent. Consequently, all the subanalyses only used these three metrics (Fig. 5 and Table 2).

The CEST effect measured is often complicated by various contributors, especially the overlapping interaction between exchangeable pools. A full description of biological tissues with the Bloch–McConnell equation is highly nonlinear and involves tens of unknown parameters, making it practically infeasible to determine the metabolic contributor to the contrast between epileptic and normal tissues. Thus, we modified a previous two-stage analysis method to explore the leading metabolic contributor,[18] which had substantially fewer unknown parameters and made the analysis tractable in practice. Among all the major exchangeable CEST pools, the amine group best explained the experimental contrast between epileptogenic and normal HA by a 25% increase in its concentration (Table 3B). Notably, the

(A) First stage	MT	Amide	Guanidinium	Amine	Hydroxyl	NOE
Fraction (%)	3.67	0.19	0.020	0.010	0.005	1.34
Exchange rate	20	45	250	1000	3000	9
(B) Second stage			**mRMSE**		**Percentage of change**	
MT fraction			0.2622		−42%	
Amide fraction			0.2671		9%	
Guanidinium fraction			0.2394		34%	
Amine fraction			0.2345		25%	
Hydroxyl fraction			0.2398		400%	
NOE fraction			0.2745		−4%	

(A) First stage: results of the 12 parameters fitted to the CESTR spectra acquired from the normal HA using the 7-pool Bloch–McConnell equation. (B) Second stage: the minimum root mean squared error (mRMSE) achieved between the simulated and experimental signals (difference of CESTR spectra between the epileptogenic and normal HA) by varying the concentration of the MT, amide, guanidinium, amine, hydroxyl, or NOE pool alone each time. The percentages of change corresponding to the mRMSE were listed in the third column. The smaller the mRMSE, the higher the possibility that the associated metabolite contributed to the experimental results observed.

Table 3: **Metabolic contributors revealed by the modified two-stage Bloch-McConnell fitting method.**

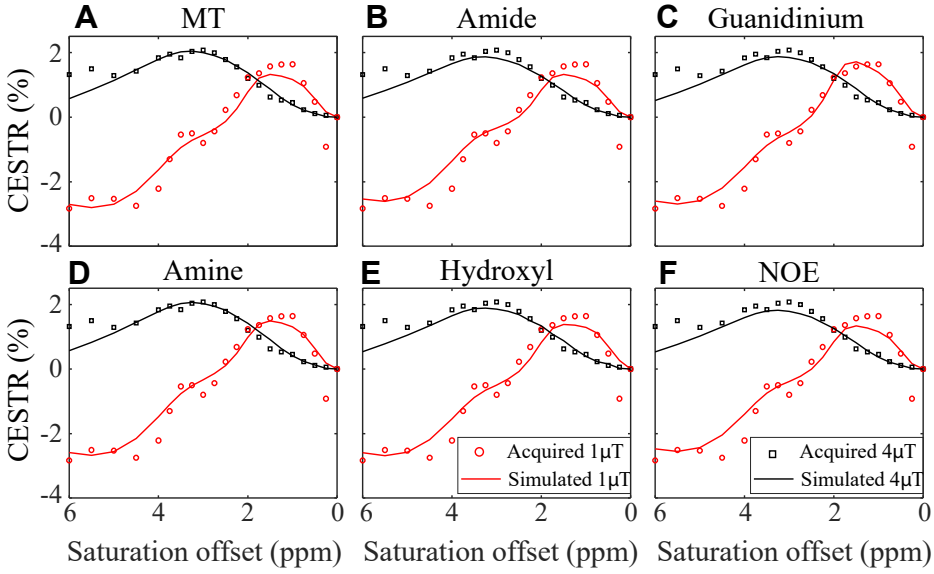

Fig. 6: **Experimental (dotted line) and simulated (solid line) CESTR spectra in the HA ipsilateral to the epileptic focus at two saturation powers (1 and 4 μT).** The CESTR curves were simulated with the normal HA parameters listed in Table 3A except for varying the concentration of the MT (**A**), amide (**B**), guanidinium (**C**), amine (**D**), hydroxyl (**E**), or NOE (**F**) pool according to Table 3B, in order to generate the minimum difference between experimental and simulated CEST contrasts. An increase of 25% in the amine concentration yielded the simulated spectra closest to the experimental ones.

amine pool originated from glutamate and proteins as reported previously.[16,35] And thus, an increased amine level was in line with the prior literature that evaluated glutamate played a critical role in generating and maintaining epilepsy.[19,20] The guanidinium moiety was the second-leading possible contributor to the CEST contrast with a 34% increase in its concentration (Table 3B), which was concordant with Lee et al.'s study[36] of raised creatine levels in epileptic rats. Although the hydroxyl pool was the third-leading candidate, it's fitting performance required a 400% increase in the concentration (Table 3B), which is too drastic a change and is unlikely to be true in the human brain. The specific molecules contributing to the CEST contrast between epileptogenic and normal HA need to be investigated in future studies.

Fluorodeoxyglucose (FDG) positron emission tomography (PET) is often used to help lateralize the seizure focus of sMRI-negative TLE. Gok et al. reported that FDG-PET could correctly lateralize 84% (32/38) of sMRI-negative patients.[37] A meta-analysis of FDG-PET on the laterality estimation found that the PET hypometabolism was concordant with the lesion side in 76.8% of sMRI-negative TLE patients.[7,38] In this study, CESTR showed promising predictive power not only in the total sample of mixed sMRI-positive/sMRI-negative patients (AUC: 0.84) but also in the subgroup of sMRI-negative patients (AUC: 0.83), which was comparable to the results reported in prior FDG-PET work. But compared with PET, MRI is radiation-free and low-cost, and thus CEST MRI has great potential to serve as a preoperative evaluation tool for TLE patients.

It was reported that FDG-PET hypometabolism often occurred beyond the mesial temporal lobe.[39] Wong et al.[40] mapped the extratemporal hypometabolism in 64 MTLE patients and demonstrated that extratemporal hypometabolism was most frequent in the ipsilateral frontal lobe (48%) and ipsilateral insula (34%). Thus, we analyzed the mean CESTR between 2.25 and 3.25 ppm in the frontal lobe, insula, and temporal lobe (including superior temporal gyrus, middle temporal gyrus, inferior temporal gyrus, and fusiform gyrus) to investigate the role of extratemporal CEST in the TLE lateralization. The ROIs and the corresponding statistics are shown in Supplementary Fig. S3. There was no significant difference in CESTR between the ipsilateral and contralateral frontal lobe, insula, or temporal lobe (p = 0.84, 0.25, and 0.53, respectively). In the future, we will conduct a more detailed segmentation of the brain, and study the prediction performance of CEST signals in all the brain regions for the TLE laterality.

There are some limitations to this study. Although the sample size of 40 is the largest in the CEST MRI field for studying TLE, all our data were collected from a single center. The study lacked post-surgical validation of seizure lateralization in all but five patients. In future studies, it is necessary to recruit more patients from different centers to further confirm the clinical value of CEST MRI in seizure lateralization. In addition, only a single-slice CEST acquisition was used, which

precluded the evaluation of metabolism in the entire hippocampus and amygdala, and might have missed parts of the lesions. Furthermore, some bias might have been introduced during the calculation of asymmetry measurements since the symmetric MRI acquisition of the two brain sides could not be guaranteed. Three-dimensional CEST imaging sequences[41] should be used to measure the entire epileptic network in future studies. In any case, this work proved the feasibility of CEST in lateralizing seizure foci of TLE at 3 Tesla, which potentially warrants more research or clinical studies of the molecular MRI technique for the preoperative assessment of epilepsy.

Contributors

KW, QW, and YZ conceptualized the study and developed the study with DCW, YCH, HYH, WW, YS, YM, and DW. KW, QW, DCW, YM, and YZ contributed to the data collection. QW and YZ verified and analyzed the data with the help of WW and HYH and performed the data visualization. YZ provided supervision. KW and YZ contributed to funding the acquisition. The original draft was written by QW and YZ, and then all the authors contributed to the revision of the manuscript and approved the final version.

Data sharing statement

All the data used to evaluate the conclusion in this study are available within the paper and its Supplementary Information. The raw MRI data of the patients and custom-written MATLAB code are available for research purposes from the corresponding author upon reasonable request.

Declaration of interests

Yi-Cheng Hsu and Yi Sun are employed by Siemens Healthcare Ltd.

Acknowledgments

We are grateful for the help from clinical coordinators, patients, and patients' families. This work was supported by the National Natural Science Foundation of China 81971605 and LY19H180006, Key R&D Program of Zhejiang Province 2022C04031, Leading Innovation and Entrepreneurship Team of Zhejiang Province 2020R01003, National Key R&D Program of China grant 2017YFC0907700, and the MOE Frontier Science Center for Brain Science & Brain-Machine Integration, Zhejiang University.

Appendix A. Supplementary data

Supplementary data related to this article can be found at https://doi.org/10.1016/j.ebiom.2023.104460.

References

1 Fiest KM, Sauro KM, Wiebe S, et al. Prevalence and incidence of epilepsy: a systematic review and meta-analysis of international studies. *Neurology*. 2017;88(3):296–303.
2 Sperling MR. The consequences of uncontrolled epilepsy. *CNS Spectr*. 2004;9(2):98–101, 6–9.
3 Blumcke I, Thom M, Aronica E, et al. International consensus classification of hippocampal sclerosis in temporal lobe epilepsy: a Task Force report from the ILAE Commission on Diagnostic Methods. *Epilepsia*. 2013;54(7):1315–1329.
4 Tatum WOt. Mesial temporal lobe epilepsy. *J Clin Neurophysiol*. 2012;29(5):356–365.
5 Ojemann GA. Treatment of temporal lobe epilepsy. *Annu Rev Med*. 1997;48:317–328.
6 Davis KA, Nanga RP, Das S, et al. Glutamate imaging (GluCEST) lateralizes epileptic foci in nonlesional temporal lobe epilepsy. *Sci Transl Med*. 2015;7(309):309ra161.
7 Muhlhofer W, Tan YL, Mueller SG, Knowlton R. MRI-negative temporal lobe epilepsy-What do we know? *Epilepsia*. 2017;58(5):727–742.
8 Thivard L, Bouilleret V, Chassoux F, et al. Diffusion tensor imaging can localize the epileptogenic zone in nonlesional extra-temporal refractory epilepsies when [18F] FDG-PET is not contributive. *Epilepsy Res*. 2011;97(1–2):170–182.
9 Struck AF, Hall LT, Floberg JM, Perlman SB, Dulli DA. Surgical decision making in temporal lobe epilepsy: a comparison of [(18)F] FDG-PET, MRI, and EEG. *Epilepsy Behav*. 2011;22(2):293–297.
10 Concha L, Kim H, Bernasconi A, Bernhardt BC, Bernasconi N. Spatial patterns of water diffusion along white matter tracts in temporal lobe epilepsy. *Neurology*. 2012;79(5):455–462.
11 Pustina D, Avants B, Sperling M, et al. Predicting the laterality of temporal lobe epilepsy from PET, MRI, and DTI: a multimodal study. *Neuroimage Clin*. 2015;9:20–31.
12 Knowlton RC, Laxer KD, Ende G, et al. Presurgical multimodality neuroimaging in electroencephalographic lateralized temporal lobe epilepsy. *Ann Neurol*. 1997;42(6):829–837.
13 Capizzano AA, Vermathen P, Laxer KD, et al. Temporal lobe epilepsy: qualitative reading of 1H MR spectroscopic images for presurgical evaluation. *Radiology*. 2001;218(1):144–151.
14 van Zijl PC, Yadav NN. Chemical exchange saturation transfer (CEST): what is in a name and what isn't? *Magn Reson Med*. 2011;65(4):927–948.
15 van Zijl PC, Lam WW, Xu J, Knutsson L, Stanisz GJ. Magnetization transfer contrast and chemical exchange saturation transfer MRI. Features and analysis of the field-dependent saturation spectrum. *Neuroimage*. 2018;168:222–241.
16 Cai K, Haris M, Singh A, et al. Magnetic resonance imaging of glutamate. *Nat Med*. 2012;18(2):302–306.
17 Zhang XY, Wang F, Xu J, Gochberg DF, Gore JC, Zu Z. Increased CEST specificity for amide and fast-exchanging amine protons using exchange-dependent relaxation rate. *NMR Biomed*. 2018;31(2):e3863.
18 Wen Q, Wang K, Hsu YC, et al. Chemical exchange saturation transfer imaging for epilepsy secondary to tuberous sclerosis complex at 3 T: Optimization and analysis. *NMR Biomed*. 2021;34(9):e4563.
19 During MJ, Spencer DD. Extracellular hippocampal glutamate and spontaneous seizure in the conscious human brain. *Lancet*. 1993;341(8861):1607–1610.
20 Olney J, Collins R, Sloviter R. Excitotoxic mechanisms of epileptic brain damage. *Adv Neurol*. 1986;44:857–877.
21 Scheffer IE, Berkovic S, Capovilla G, et al. ILAE classification of the epilepsies: position paper of the ILAE Commission for Classification and Terminology. *Epilepsia*. 2017;58(4):512–521.
22 Mugler JP, Brookeman JR. Three-dimensional magnetization-prepared rapid gradient-echo imaging (3D MP RAGE). *Magn Reson Med*. 1990;15(1):152–157.
23 Hajnal JV, Bryant DJ, Kasuboski L, et al. Use of fluid attenuated inversion recovery (FLAIR) pulse sequences in MRI of the brain. *J Comput Assist Tomogr*. 1992;16(6):841–844.
24 Kim M, Gillen J, Landman BA, Zhou J, van Zijl PC. Water saturation shift referencing (WASSR) for chemical exchange saturation transfer (CEST) experiments. *Magn Reson Med*. 2009;61(6):1441–1450.
25 Liu R, Zhang H, Niu W, et al. Improved chemical exchange saturation transfer imaging with real-time frequency drift correction. *Magn Reson Med*. 2019;81(5):2915–2923.
26 Heo HY, Lee DH, Zhang Y, et al. Insight into the quantitative metrics of chemical exchange saturation transfer (CEST) imaging. *Magn Reson Med*. 2017;77(5):1853–1865.
27 Ferran Prados MJC, Burgos N, Wheeler-Kingshott CAM, Ourselin S. *NiftyWeb: web based platform for image processing on the cloud*. Singapore: International Society for Magnetic Resonance in Medicine (ISMRM) 24th Scientific Meeting and Exhibition; 2016.
28 Winston GP, Cardoso MJ, Williams EJ, et al. Automated hippocampal segmentation in patients with epilepsy: available free online. *Epilepsia*. 2013;54(12):2166–2173.
29 Mori S, Wu D, Ceritoglu C, et al. MRICloud: delivering high-throughput MRI neuroinformatics as cloud-based software as a service. *Comput Sci Eng*. 2016;18(5):21–35.
30 Wu T, Chen D, Chen Q, et al. Automatic lateralization of temporal lobe epilepsy based on MEG network features using support vector machines. *Complexity*. 2018:1–10.
31 Winston GP, Vos SB, Burdett JL, Cardoso MJ, Ourselin S, Duncan JS. Automated T2 relaxometry of the hippocampus for temporal lobe epilepsy. *Epilepsia*. 2017;58(9):1645–1652.
32 Despotovic I, Goossens B, Philips W. MRI segmentation of the human brain: challenges, methods, and applications. *Comput Math Methods Med*. 2015;2015:450341.

33 Liao C, Wang K, Cao X, et al. Detection of lesions in mesial temporal lobe epilepsy by using MR fingerprinting. *Radiology*. 2018;288(3):804–812.
34 Soma T, Momose T, Takahashi M, et al. Usefulness of extent analysis for statistical parametric mapping with asymmetry index using inter-ictal FGD-PET in mesial temporal lobe epilepsy. *Ann Nucl Med*. 2012;26(4):319–326.
35 Cui J, Zu Z. Towards the molecular origin of glutamate CEST (GluCEST) imaging in rat brain. *Magn Reson Med*. 2020;83(4):1405–1417.
36 Lee DH, Lee DW, Kwon JI, et al. In vivo mapping and quantification of creatine using chemical exchange saturation transfer imaging in rat models of epileptic seizure. *Mol Imaging Biol*. 2019;21(2):232–239.
37 Gok B, Jallo G, Hayeri R, Wahl R, Aygun N. The evaluation of FDG-PET imaging for epileptogenic focus localization in patients with MRI positive and MRI negative temporal lobe epilepsy. *Neuroradiology*. 2013;55(5):541–550.
38 Willmann O, Wennberg R, May T, Woermann F, Pohlmann-Eden B. The contribution of 18F-FDG PET in preoperative epilepsy surgery evaluation for patients with temporal lobe epilepsy: a meta-analysis. *Seizure*. 2007;16(6):509–520.
39 Sperling MR, Gur RC, Alavi A, et al. Subcortical metabolic alterations in partial epilepsy. *Epilepsia*. 1990;31(2):145–155.
40 Wong CH, Bleasel A, Wen L, et al. The topography and significance of extratemporal hypometabolism in refractory mesial temporal lobe epilepsy examined by FDG-PET. *Epilepsia*. 2010;51(8):1365–1373.
41 Zhang Y, Yong X, Liu R, et al. Whole-brain chemical exchange saturation transfer imaging with optimized turbo spin echo readout. *Magn Reson Med*. 2020;84(3):1161–1172.